Physica A 419 (2015) 487–497

Contents lists available at ScienceDirect

Physica A

journal homepage: www.elsevier.com/locate/physa

Pattern formation and Turing instability in an activator–inhibitor system with power-law coupling

F.A. dos S. Silva, R.L. Viana *, S.R. Lopes

Department of Physics, Federal University of Paraná, 81531-990, Curitiba, Paraná, Brazil

HIGHLIGHTS

- Activator–inhibitor systems with non-local coupling are studied in two dimensions.
- Linear stability analysis of spatial modes gives conditions for Turing instability.
- Numerical simulations are performed to study non-linear saturation of linearly growing modes.

ARTICLE INFO

Article history:
Received 29 September 2014
Available online 16 October 2014

Keywords:
Reaction–diffusion systems
Activator–inhibitor systems
Non-local couplings
Pattern formation
Spatio-temporal dynamics

ABSTRACT

We investigate activator–inhibitor systems in two spatial dimensions with a non-local coupling, for which the interaction strength decreases with the lattice distance as a power-law. By varying a single parameter we can pass from a local (Laplacian) to a global (all-to-all) coupling type. We derived, from a linear stability analysis of the Fourier spatial modes, a set of conditions for the occurrence of a Turing instability, by which a spatially homogeneous pattern can become unstable. In nonlinear systems the growth of these modes is limited and pattern formation is possible. We have studied some qualitative features of the patterns formed in non-local coupled activator–inhibitor systems described by the Meinhardt–Gierer equations.

1. Introduction

One of the key questions in morphogenesis is how a single egg develops into a complex organism. Since all the cells belonging to the egg share an identical genetic code, some mechanism should account for the fact that the cells eventually become different from each other [1]. Translating this question into a mathematical language, this means how a spatially homogeneous pattern evolves into an inhomogeneous one [2]. Other biological examples of pattern formation are the skin pigmentation of animals, colony formation of small marine animals, and the regular spacing of leaves in a plant [3].

Minimal models aiming to mimic these and other related phenomena consist of two substances: one activator and one inhibitor. The pattern that is formed results from the interplay between the concentrations of these substances, whose spatio-temporal evolution is governed by coupled reaction–diffusion systems (activator–inhibitor models). In 1952 Alan Turing addressed this question from a linear stability analysis and found that a stable homogeneous pattern can become unstable (the so-called Turing instability) if the inhibitor diffuses more rapidly than the activator. In other words, if the diffusion coefficient of the inhibitor is greater than that of the activator by a given factor [4].

In activator–inhibitor models this factor can be as large as 10. Since the diffusion coefficient of most ions in water has nearly the same value ($circa 10^{-9}$ m^2/s), the production of Turing instability in the laboratory is a difficult task. A major

* Corresponding author.
E-mail address: viana@fisica.ufpr.br (R.L. Viana).

http://dx.doi.org/10.1016/j.physa.2014.09.059
0378-4371/

progress was the observation that the introduction of a third substance fixed to a matrix in the solution can create a large difference between the diffusion coefficients of the activator and the inhibitor, since one of them binds reversibly to the immobile molecule and has an effectively smaller diffusion coefficient, in comparison with the substance which does not bind [5]. Indeed, the Turing instability has been observed in the Chlorine Dioxide–Iodine–Malonic Acid (CDIMA) reaction, for which the third substance was a starch indicator embedded in a gel matrix [6,7].

The simple existence of a Turing instability, however, is not sufficient *per si* to explain pattern formation. Since there is a strong positive feedback on the increase of the activator, there would be an unlimited increase of the latter. The presence of nonlinearities in the local dynamics, for example due to the inhibitor concentration, saturates the Turing instability into a stable and spatially inhomogeneous pattern. A model showing this kind of behavior was proposed by Meinhardt and Gierer and remains a paradigm for studies of activator–inhibitor systems [8–10].

Gierer and Meinhardt have shown that stable inhomogeneous patterns can be formed if the auto-catalytic production of the activator is short-ranged, while the formation of the inhibitor is long-ranged. In other words, the self-enhancing process involving the activator is chiefly local, whereas the inhibitor should have a long-range behavior characterized by rapid spreading, producing activator removal at long distances [11].

The role of the diffusion range is thus of central importance in the dynamics of activator–inhibitor systems. On the other hand, the mathematical modeling of reaction–diffusion equation involves Laplacian coupling, represented by second-order spatial derivatives. Such models are derived from a mass balance and Fick's law (the diffusion flux points from large to small concentration regions). However, in this class of models, the coupling is nevertheless of a local nature, characterized by interactions with the nearest-neighbor sites in a discrete lattice.

In this paper we present a more general formulation for the activator–inhibitor system, characterized by a non-local coupling: a lattice site can interact essentially with all its neighbors. The strength of this coupling is supposed to decrease with the lattice distance as a power-law, where a range parameter is introduced that can be varied so as to pass from a global (all-to-all) coupling to a local (nearest-neighbor) one [12–14].

We have previously described one-dimensional chains of nonlinear oscillators coupled according to this type nonlocal interaction [15]. In that work we found that global couplings spread information among oscillators more rapidly than local couplings, in such a way that globally coupled oscillators are less likely to present a Turing instability than locally coupled ones. Moreover, collective phenomena like frequency synchronization [16] are more likely to occur in the global case than in the local coupling [15].

However the one-dimensional case is rather idealized since spatio-temporal patterns of interest are typically two-dimensional, such as those observed in skin pigmentation, chemical cells, etc. In the present paper we investigate the occurrence of a Turing instability in a two-dimensional system of nonlocally coupled oscillators. We used a linear stability analysis to study the role of the effective range and the diffusion coefficients on the conditions for the occurrence of a Turing instability [17]. We also performed numerical simulations of the coupled system so as to investigate pattern formation and its dependence with range and diffusion.

This paper is organized as follows: in Section 2 we introduce the system of non-locally coupled activator–inhibitor oscillators and explore its limiting cases. Section 3 is devoted to the linear analysis of Fourier mode stability leading to conditions for the Turing instability involving both the range parameter and diffusion coefficients. In Section 4 we consider pattern formation for the Meinhardt–Gierer model of activator–inhibitor oscillators with power-law coupling. Our Conclusions are left to the final section.

2. Non-locally coupled oscillators

Activator–inhibitor systems with local coupling are usually described by coupled reaction–diffusion equations:

$$\frac{\partial u}{\partial t} = f(u, v) + D_u \nabla^2 u, \tag{1}$$

$$\frac{\partial v}{\partial t} = g(u, v) + D_v \nabla^2 v, \tag{2}$$

where $u(\mathbf{r}, t)$ and $v(\mathbf{r}, t)$ denote the local concentrations of the activator and inhibitor species, respectively. The functions $f(u, v)$ and $g(u, v)$ stand for the local dynamics of the system, in which the activator auto-catalytically enhances its own production and the inhibitor suppresses the activator growth [18]. The diffusion constants of the activator and inhibitor species are denoted, respectively, by D_u and D_v, and we assume them to be positive-defined.

A spatially homogeneous pattern becomes linearly unstable (Turing instability) if the ratio of the diffusion constants D_v/D_u exceeds a threshold value. The nonlinear terms in f and g, however, saturate the linear growth and produce a spatially inhomogeneous pattern, in which there are domains with high and low values of the activator concentration, with respect to a uniform background.

In the following, we will consider two-dimensional patterns in the x and y directions, along which we make a coarse-grained description of the spatial patterns. For a square lattice with local coupling, we link a given site to its nearest neighbors in both directions. There are N^2 cells of area Δ^2 and the variables are discretized as

$$u_{k,j}(t) = u(x = k\Delta, y = j\Delta; t), \qquad v_{k,j}(t) = v(x = k\Delta, y = j\Delta; t), \tag{3}$$

with $k, j = 0, 1, \ldots (N-1)$ and periodic boundary conditions. The discretized Laplacian for the activator species in (1)–(2) is

$$\nabla^2 u_{k,j} = \frac{1}{\Delta^2}\left(u_{k-1,j} + u_{k+1,j} + u_{k,j-1} + u_{k,j+1} - 4u_{k,j}\right), \tag{4}$$

with a similar expression for the inhibitor species, such that the equations for the locally coupled activator–inhibitor system are

$$\frac{\mathrm{d}u_{k,j}}{\mathrm{d}t} = f(u_{k,j}, v_{k,j}) + \frac{D_u}{4}\left(u_{k+1,j} + u_{k-1,j} + u_{k,j+1} + u_{k,j-1} - 4u_{k,j}\right), \tag{5}$$

$$\frac{\mathrm{d}v_{k,j}}{\mathrm{d}t} = g(u_{k,j}, v_{k,j}) + \frac{D_v}{4}\left(v_{k+1,j} + v_{k-1,j} + v_{i,k+1} + v_{i,k-1} - 4v_{k,j}\right). \tag{6}$$

Let us now consider the case in which the coupling is non-local, i.e. the diffusion flux does not depend only on the local gradient of the activator and inhibitor concentrations. In terms of the lattice description this means that the coupling between oscillators is no longer restricted to the nearest neighbors but instead takes into account a wider vicinity which eventually can encompass the entire lattice. A general way to express this non-local coupling is to replace (1)–(2) by the following integro-differential equations:

$$\frac{\partial u}{\partial t} = f(u, v) + D_u \int d^2\mathbf{r}'\sigma(\mathbf{r}, \mathbf{r}')u(\mathbf{r}', t), \tag{7}$$

$$\frac{\partial v}{\partial t} = g(u, v) + D_v \int d^2\mathbf{r}'\sigma(\mathbf{r}, \mathbf{r}')v(\mathbf{r}', t), \tag{8}$$

where $\sigma(\mathbf{r}, \mathbf{r}')$ is a non-local interaction kernel describing the interaction of a given lattice point with its distant neighbors, thus exhibiting a dependence with the distance along the lattice.

In models where the coupling between oscillators is mediated by a chemical diffusing through the medium where the oscillators are embedded such interaction decays exponentially with the distance [19]. Another possibility is a power-law decay, for which the interaction strength between the lattice points depends on their mutual distance in a power-law fashion, with an exponent $\alpha > 0$ [12–14]. In this paper we adapt the locally coupled two-dimensional square lattice to include such a non-local coupling through a power-law prescription in the following form:

$$\frac{\mathrm{d}u_{k,j}}{\mathrm{d}t} = f(u_{k,j}, v_{k,j}) - D_u u_{k,j} + \frac{D_u}{\kappa(\alpha)} \sum_{r=-N'}^{N'}{}^{\star} \sum_{\ell=-N'}^{N'}{}^{\star} \frac{u_{k+r,j+\ell}}{(r^2+\ell^2)^{\alpha/2}}, \tag{9}$$

$$\frac{\mathrm{d}v_{k,j}}{\mathrm{d}t} = g(u_{k,j}, v_{k,j}) - D_v v_{k,j} + \frac{D_v}{\kappa(\alpha)} \sum_{r=-N'}^{N'}{}^{\star} \sum_{\ell=-N'}^{N'}{}^{\star} \frac{v_{k+r,j+\ell}}{(r^2+\ell^2)^{\alpha/2}}, \tag{10}$$

where $N' = (N-1)/2$, with N odd, and the starred summations mean that we *exclude from them those terms with* $r = \ell = 0$. The normalization factor is

$$\kappa(\alpha) = \sum_{r=-N'}^{N'}{}^{\star} \sum_{\ell=-N'}^{N'}{}^{\star} \frac{1}{(r^2+\ell^2)^{\alpha/2}}. \tag{11}$$

Moreover we assume periodic boundary conditions

$$u_{k\pm N, j\pm N} = u_{k,j}, \qquad v_{k\pm N, j\pm N} = v_{k,j}, \tag{12}$$

such that the square lattice becomes a 2-torus.

It is instructive to explore the limiting cases of this non-local coupling prescription. If we let α tend to infinity there follows that $\kappa \to 4$ and, in the summations (9)–(10) only those terms with $r =$ and $\ell = 1$ survive, such that we obtain Eqs. (5)–(6) for the locally coupled oscillators. On the other hand, if $\alpha = 0$ we obtain $\kappa = N^2 - 1$, and the interaction strength does not depend on the lattice distance. The summations in (9)–(10) can be rearranged as to yield

$$\frac{\mathrm{d}u_{k,j}}{\mathrm{d}t} = f(u_{k,j}, v_{k,j}) - D_u\left(\overline{\overline{u}}_{k,j} - u_{k,j}\right), \tag{13}$$

$$\frac{\mathrm{d}v_{k,j}}{\mathrm{d}t} = g(u_{k,j}, v_{k,j}) - D_v\left(\overline{\overline{v}}_{k,j} - v_{k,j}\right), \tag{14}$$

where the double bars denote the average value of the activator and inhibitor concentrations at each lattice point, except for the values at the point itself:

$$\overline{\overline{u}}_{k,j} = \frac{1}{N^2-1} \sum_{r=-N'}^{N'}{}^{\star} \sum_{\ell=-N'}^{N'}{}^{\star} u_{k+r,j+\ell}, \tag{15}$$

$$\overline{\overline{v}}_{k,j} = \frac{1}{N^2-1} \sum_{r=-N'}^{N'}{}^{\star} \sum_{\ell=-N'}^{N'}{}^{\star} v_{k+r,j+\ell}. \tag{16}$$

Note that these averages are different for each lattice point. Hence in the limit $\alpha = 0$ we have a kind of global (all-to-all) coupling, where each oscillator interacts with the "mean field" generated by all the other oscillators.

In general, for arbitrary α, we have an intermediate kind of coupling that interpolates between these two limiting cases. We remark that, in the thermodynamic limit ($N \to \infty$), the summations in the normalization factor (11) do not converge for $0 < \alpha < 1$. For finite lattices, however, all values of α are allowed.

3. Turing instability

3.1. Linear stability analysis

We begin by considering a linear model for the local dynamics of the uncoupled activator–inhibitor system

$$f(u, v) = a\,u + b\,v, \tag{17}$$

$$g(u, v) = c\,u + d\,v, \tag{18}$$

where a, b, c and d are coefficients, which may be interpreted as the elements of the Jacobian matrix of a non-linear system, evaluated at an equilibrium point. We assume that all the oscillators are identical, i.e. the values of these coefficients are the same for all oscillators. This assumption is valid as long as the system parameters remain uniform over the domain of interest, i.e. there are no inhomogeneities in the parameters of the system. Since the oscillators are identical, the equilibrium state at the origin also holds for each oscillator belonging to the coupled system (9)–(10).

Actually the values of the activator and inhibitor concentrations (u and v, respectively) should be meant as deviations of their background values u_0 and v_0. Hence the equilibrium (0, 0) corresponds to a spatially homogeneous state with constant concentrations of both activator and inhibitor species. If this homogeneous state is linearly stable against small perturbations we demand that the equilibrium (0, 0) be asymptotically stable, what amounts to the following conditions [20]

$$ad - bc > 0, \qquad a + d < 0. \tag{19}$$

Considering now the coupling effect for a non-local prescription with α arbitrary, we are interested to determine for which values of the diffusion coefficients (or their ratio) this spatially homogeneous state loses stability. We use Fourier transforms for the state variables ($k, j = 0, 1, 2, \ldots, N-1$):

$$u_{k,j}(t) = \sum_{m=0}^{N-1} \sum_{n=0}^{N-1} \xi_{m,n}(t) \mathrm{e}^{2\pi \mathrm{i}(mk+nj)/N}, \tag{20}$$

$$v_{k,j}(t) = \sum_{m=0}^{N-1} \sum_{n=0}^{N-1} \eta_{m,n}(t) \mathrm{e}^{2\pi \mathrm{i}(mk+nj)/N}, \tag{21}$$

where ξ_{mn} and η_{mn} are the corresponding Fourier coefficients. Substituting (20)–(21) into (9)–(10), there follows that these coefficients obey the following linear evolution equations

$$\frac{\mathrm{d}\xi_{m,n}}{\mathrm{d}t} = a_\sigma\,\xi_{m,n} + b\,\eta_{m,n}, \tag{22}$$

$$\frac{\mathrm{d}\eta_{m,n}}{\mathrm{d}t} = c\,\xi_{m,n} + d_\sigma\,\eta_{m,n}, \tag{23}$$

where

$$a_\sigma \equiv a - 2D_u\sigma_{m,n}(\alpha), \tag{24}$$

$$d_\sigma \equiv d - 2D_v\sigma_{m,n}(\alpha), \tag{25}$$

$$\sigma_{m,n}(\alpha) \equiv \frac{1}{2} - \frac{1}{\kappa(\alpha)} \left[\sum_{r=1}^{N'} \frac{1}{r^\alpha} \cos\left(\frac{2\pi mr}{N}\right) + \sum_{\ell=1}^{N'} \frac{1}{\ell^\alpha} \cos\left(\frac{2\pi n\ell}{N}\right) + 2 \sum_{r=1}^{N'} \sum_{\ell=1}^{N'} \frac{1}{(r^2+\ell^2)^{\alpha/2}} \cos\left(\frac{2\pi mr}{N}\right) \cos\left(\frac{2\pi n\ell}{N}\right) \right]. \tag{26}$$

The function $\sigma_{m,n}(\alpha)$ plays a key role in the stability of the homogeneous state. Fig. 1 shows its graph as a function of the variables m/N and n/N, which vary from 0 to 1, as both m and n go from 0 to $N-1$. For $\alpha = 0$ the function is essentially a

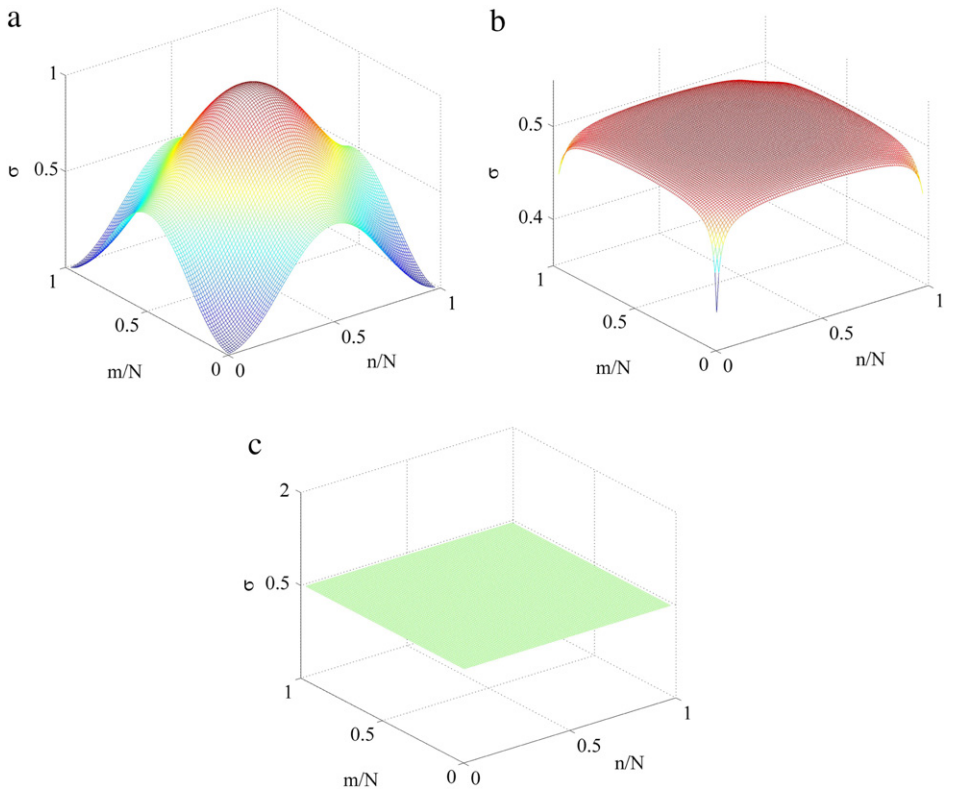

Fig. 1. (Color online) The function $\sigma_{m,n}(\alpha)$ as a function of m/N and n/N for $N = 101$ and (a) $\alpha = 1000$ (b) 1, and (c) and 0.

constant plateau at $\sigma \approx 0.5$ (Fig. 1(c)). In fact, letting $\alpha \to 0$ in (26) gives

$$\sigma_{m,n}(\alpha = 0) = \begin{cases} 0 & \text{if } m = 0 \text{ and } n = 0, \\ \dfrac{1}{2}\dfrac{N^2}{N^2 - 1} & \text{otherwise.} \end{cases} \tag{27}$$

For large N the value of $\sigma_{m,n}(0)$ approaches $1/2$, indeed.

Intermediate values of α, for which the coupling is non-local but its strength depends on the lattice distance, show a pronounced plateau near $\sigma = 1/2$, with a fast decay to zero near the boundaries of both axes (Fig. 1(b)). Finally, for large α we have a double sinusoidal function, peaked at a value $\sigma_{\max} = 1$ (Fig. 1(a)), what can be inferred from taking the limit $\alpha \to \infty$ in (26), what results in

$$\sigma_{m,n}(\alpha \to \infty) = \frac{1}{2}\left[\sin^2\left(\frac{2\pi m}{N}\right) + \sin^2\left(\frac{2\pi n}{N}\right)\right]. \tag{28}$$

For arbitrary α it turns out that the values taken on by the function σ have upper and lower bounds:

$$0 \le \sigma_{m,n}(\alpha) \le \sigma_{\max}(\alpha), \quad \text{with } 0 \le \sigma_{\max}(\alpha) \le 1, \tag{29}$$

$$\sigma_{\min}(\alpha) \le \sigma_{m,n}(\alpha) \le 1, \quad \text{with } 0 \le \sigma_{\min}(\alpha) \le 1. \tag{30}$$

The upper bound $\sigma_{\max}$ is plotted in Fig. 2(a) as a function of α for different values of N (the total number of oscillators being N^2), showing that it varies from 0.5 to 1.0 as we pass from a global to a local coupling. The effect of increasing number of oscillators is illustrated by Fig. 2(b), where we plot $\sigma_{\max}$ against N, showing that for $N \gtrsim 50$ we have already achieved saturation values.

The linear equations for the Fourier coefficients (22)–(23) have also an equilibrium at the origin (0, 0), which corresponds to a spatially homogeneous pattern. The stability of this pattern, taking into account the coupling among oscillators, can be obtained by considering the stability conditions for the equilibrium point in Fourier space, which are similar to the ones given by Eq. (19), namely

$$q_\sigma \equiv a_\sigma d_\sigma - bc > 0, \tag{31}$$

$$a_\sigma + d_\sigma < 0. \tag{32}$$

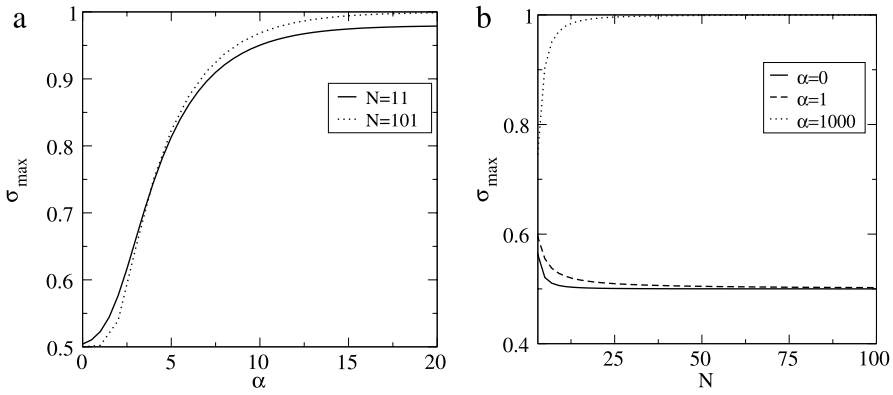

Fig. 2. Upper bound of the σ function as a function of (a) the range parameter and (b) lattice size.

It concludes that the conditions for a Turing instability, i.e. when the spatially homogeneous state loses stability under small deviations of homogeneity, are

$$4D_uD_v\sigma^2_{m,n}(\alpha) - 2\sigma_{m,n}(\alpha)(a\,D_v + d\,D_u) + q < 0. \tag{33}$$

This inequality is fulfilled by values of $\sigma_{mn}(\alpha)$ such that $\sigma_- < \sigma_{mn}(\alpha) < \sigma_+$, where

$$\sigma_\pm = \frac{1}{4}\left(P \pm \sqrt{P^2 - 4Q}\right), \tag{34}$$

$$Q = \frac{ad - bc}{D_u\,D_v}, \tag{35}$$

$$P = \frac{a}{D_u} + \frac{d}{D_v}. \tag{36}$$

The interpretation of the inequality (33) can be done in two ways: (i) what are the conditions on the system parameters (in particular, the diffusion coefficients) that yield a Turing instability; (ii) what normal modes (m, n) are linearly instable due to the coupling. In this paper we will consider only the former interpretation.

3.2. Parameter space

Since $0 \leq \sigma_- \leq \sigma_{\max}(\alpha) \leq 1$ it follows that

$$0 \leq P - \sqrt{P^2 - 4Q} \leq 4\sigma_{\max}(\alpha), \tag{37}$$

which implies three conditions for the occurrence of a Turing instability involving the auxiliary quantities P and Q:

$$Q > 0, \tag{38}$$

$$P > 2\sqrt{Q}, \quad \text{if } 0 \leq P \leq 4\sigma_{\max}(\alpha), \tag{39}$$

$$P > \frac{Q}{2\sigma_{\max}(\alpha)} + 2\sigma_{\max}(\alpha), \quad \text{if } P > 4\sigma_{\max}(\alpha), \tag{40}$$

which are essentially the same conditions that we have previously obtained for the case of a one-dimensional lattice of non-locally coupled oscillators [15].

The conditions above assume particularly simple forms in the two limiting cases: (i) for local coupling ($\alpha \to \infty$) we have $\sigma_{\max} = 1$ (see Eq. (28)) and we thus have

$$Q > 0, \tag{41}$$

$$P > 2\sqrt{Q}, \quad \text{if } 0 \leq P \leq 4, \tag{42}$$

$$P > \frac{Q}{2} + 2, \quad \text{if } P > 4; \tag{43}$$

(ii) for global coupling ($\alpha = 0$) the conditions (38)–(40) reduce to only one inequality:

$$P > \frac{Q}{2\sigma(0)} + 2\sigma(0), \tag{44}$$

where

$$P - \sqrt{P^2 - 4Q} < \sigma(0) < P + \sqrt{P^2 - 4Q}. \tag{45}$$

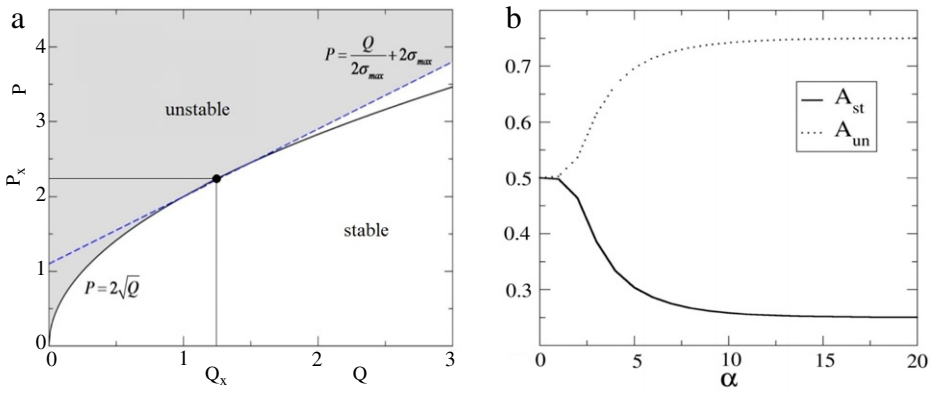

Fig. 3. (Color online) (a) Parameter plane (P, Q) for the linear stability of the homogeneous pattern. (b) Normalized stable and unstable areas in (a) as a function of α.

Since, for large N, we have from Eq. (27) that $\sigma(0) \approx 1/2$, the condition for the occurrence of a Turing instability in the globally coupled case is simply $P > Q + 1$.

For the intermediate case $\alpha = 1$, the conditions (39) and (40) can be represented, in the parameter plane (P, Q) depicted in Fig. 3(a), by solid and dashed lines, respectively, which have a single common point X whose coordinates are $(Q_X, P_X) = (4\sigma^2_{\max}(1), 4\sigma_{\max}(1))$. Since, from Fig. 2(a), $\sigma_{\max}(1) \approx 0.5$ this point is close to $(P, Q) = (1, 2)$. The parameter values yielding the Turing instability correspond to points above the curve (39) for $Q < Q_X$ and above the curve (40) for $Q > Q_X$. Conversely, the area below those curves corresponds to the stable regions.

Let $Q_0 > Q_X$ be an arbitrary value of Q. It is possible to obtain by direct integration the stable area

$$A_{\text{stable}} = \frac{1}{4\sigma_{\max}(\alpha)} + \frac{2(Q_0 - 2)}{Q_0^2}\,\sigma_{\max}(\alpha) + \frac{32}{3Q_0^2}\,\sigma^{3/2}_{\max}(\alpha) - \frac{8}{Q_0^2}\,\sigma^2_{\max}(\alpha). \tag{46}$$

Letting $Q_0 \to \infty$ then yields $A_{\text{stable}} = 1/(4\sigma_{\max}(\alpha))$. In Fig. 3(b) we plot the values of A_{stable} and $A_{unstable} = 1 - A_{\text{stable}}$ as functions of the range parameter α. For global couplings $\alpha \gtrsim 0$ both regions have equal sizes, whereas for local couplings the stable area is significantly shorter than the unstable region. In fact, for large lattices we have $\sigma_{\max} \approx 1/2$ for $\alpha = 0$ (global coupling) and $\sigma_{\max} = 1$ for large α (local coupling). Then the stable area is $A_{\text{stable}}(\alpha \to \infty) = 1/4$ and $A_{\text{stable}}(\alpha = 0) \approx 1/2$, in agreement with Fig. 3(b).

4. A dynamical model for evolving spatial patterns

4.1. Equilibria and linear stability

In this work we study a nonlinear activator–inhibitor dynamical system proposed by Meinhardt and Gierer [8,10] as a model for pattern formation related to skin pigmentation:

$$f(u, v) = \rho_u \frac{u^2}{v} - \mu_u\, u, \tag{47}$$

$$g(u, v) = \rho_v u^2 - \mu_v\, v, \tag{48}$$

where u and v are the concentrations of the activator and inhibitor substances, as before. The activator production and degradation rates are denoted by ρ_u and μ_u, respectively, whereas ρ_v and μ_v are the corresponding rates for the inhibitor species.

The activator undergoes an auto-catalytic reaction, its time rate being thus proportional to the square of its concentration (u^2) at a given time. The inhibition is represented by the v^{-1} dependence on the reaction rate. The term $-\mu_u u$ stands for the activator degradation. Moreover, the inhibitor reaction rate increases with the activator concentration, i.e. it is also influenced by its auto-catalytic process and decreases due to degradation.

The equilibrium points for Eqs. (47)–(48) satisfy

$$f(u^*, v^*) = g(u^*, v^*) = 0, \tag{49}$$

what yields two equilibria: one is the origin and another is

$$u^* = \frac{\rho_u}{\rho_v}\frac{\mu_v}{\mu_u}, \qquad v^* = \frac{\rho_u^2}{\rho_v}\frac{\mu_v}{\mu_u^2}, \tag{50}$$

on which we shall focus our attention.

The Jacobian matrix of the system (47)–(48), evaluated at the equilibrium point (50), is

$$\mathbf{J}(u^*, v^*) = \begin{pmatrix} a & b \\ c & d \end{pmatrix} = \begin{pmatrix} \mu_u & -\mu_u^2/\rho_u \\ 2\rho_u\mu_v/\mu_u & -\mu_v \end{pmatrix}, \tag{51}$$

such that the equilibrium is stable if (cf. Eq. (19)) $\mu_u < \mu_v$ and $\mu_u\mu_v > 0$. In the following we shall fix the values as $\rho_u = 0.01$, $\rho_v = 0.02$, $\mu_u = 0.01$, and $\mu_v = 0.02$ such that the equilibrium at the origin is unstable, whereas the second equilibrium point, viz. $(x^*, y^*) = (1, 1)$, is asymptotically stable.

We now consider the spatio-temporal evolution of a two-dimensional lattice, in which each site represents an activator–inhibitor system, and where the coupling is non-local, such that the interaction strength among sites decreases with the lattice distance in a power-law fashion, as in (9)–(10):

$$\frac{\mathrm{d}u_{k,j}}{\mathrm{d}t} = \rho_u \frac{u_{k,j}^2}{v_{k,j}} - \mu_u\, u_{k,j} - D_u u_{k,j} + \frac{D_u}{\kappa(\alpha)} \sum_{r=-N'}^{N'}{}^{\star} \sum_{\ell=-N'}^{N'}{}^{\star} \frac{u_{k+r,j+\ell}}{(r^2+\ell^2)^{\alpha/2}}, \tag{52}$$

$$\frac{\mathrm{d}v_{k,j}}{\mathrm{d}t} = \rho_v u_{k,j}^2 - \mu_v\, v_{k,j} - D_v v_{k,j} + \frac{D_v}{\kappa(\alpha)} \sum_{r=-N'}^{N'}{}^{\star} \sum_{\ell=-N'}^{N'}{}^{\star} \frac{v_{k+r,j+\ell}}{(r^2+\ell^2)^{\alpha/2}}, \tag{53}$$

where the normalization is given by (11). As in the linear case, we assume that the production and degradation rates, as well as the diffusion coefficients, are spatially uniform, i.e. they take on the same values for all lattice points.

The equilibria we found for the uncoupled oscillators are also fixed points for homogeneous patterns of the coupled lattice (52)–(53). Let such patterns be denoted by

$$u_{k,j}^* = u^*, \qquad v_{k,j}^* = v^*, \quad \forall\, k, j = 0, \ldots, N-1. \tag{54}$$

Hence

$$f(u^*, v^*) - D_u u^* + \frac{D_u}{\kappa(\alpha)} u^* \sum_{r=-N'}^{N'}{}^{\star} \sum_{\ell=-N'}^{N'}{}^{\star} \frac{1}{(r^2+\ell^2)^{\alpha/2}} = 0,$$

$$g(u^*, v^*) - D_v v^* + \frac{D_v}{\kappa(\alpha)} v^* \sum_{r=-N'}^{N'}{}^{\star} \sum_{\ell=-N'}^{N'}{}^{\star} \frac{1}{(r^2+\ell^2)^{\alpha/2}} = 0,$$

because of (49) and (11).

We shall focus our attention on the second equilibrium point (50). By redefining variables as $u' = u - u^*$ and $v' = v - v^*$ we displace this point to the origin and can use the linear stability analysis for the coupled system. In the latter, the relevant parameters are P and Q, here given by

$$P = \frac{\mu_u}{D_u} - \frac{\mu_v}{D_v}, \qquad Q = \frac{\mu_u}{D_u}\frac{\mu_v}{D_v}. \tag{55}$$

According to (38)–(40), the equilibrium is Turing-unstable if the following conditions are fulfilled in the case $\alpha \neq 0$:

$$\frac{\mu_u}{D_u}\frac{\mu_v}{D_v} > 0, \tag{56}$$

$$\mu_u D_v - \mu_v D_u > 2D_u D_v \sqrt{\mu_u\mu_v/D_u D_v}, \quad \text{if } 0 \le \mu_u D_v - \mu_v D_u \le 4D_u D_v \sigma_{\max}, \tag{57}$$

$$\mu_u D_v - \mu_v D_u > \mu_u\mu_v/(2\sigma_{\max}) + 2\sigma_{\max} D_u D_v, \quad \text{if } \mu_u D_v - \mu_v D_u > 4D_u D_v \sigma_{\max}(\alpha). \tag{58}$$

The case $\alpha = 0$ needs a separate analysis and the result is

$$\mu_u D_v - \mu_v D_u > \mu_u\mu_v + D_u D_v. \tag{59}$$

Since (56) is trivially satisfied, on keeping the system parameters constant except for the diffusion coefficients, (57) and (58) determine for which values of D_u and D_v the spatially homogeneous and stable pattern undergoes a Turing instability.

4.2. Numerical results

The N^2 coupled differential equations (52)–(53) were numerically integrated using the LSODA package, based on a 12th-order Adams predictor–corrector method. We keep the inhibitor diffusion coefficient fixed at $D_v = 0.2$ and take, as our control parameters, the activator diffusion coefficient D_u and the range parameter α. We integrated the coupled equations for $N^2 = 10\,201$ lattice sites, with periodic boundary conditions and randomly chosen initial conditions. The integration was carried on by a time large enough to yield a stationary pattern – we stopped the integration when two consecutive spatial patterns differ by a quantity less than a specified tolerance of 10^{-5} – a condition typically achieved after 2×10^5 integration steps.

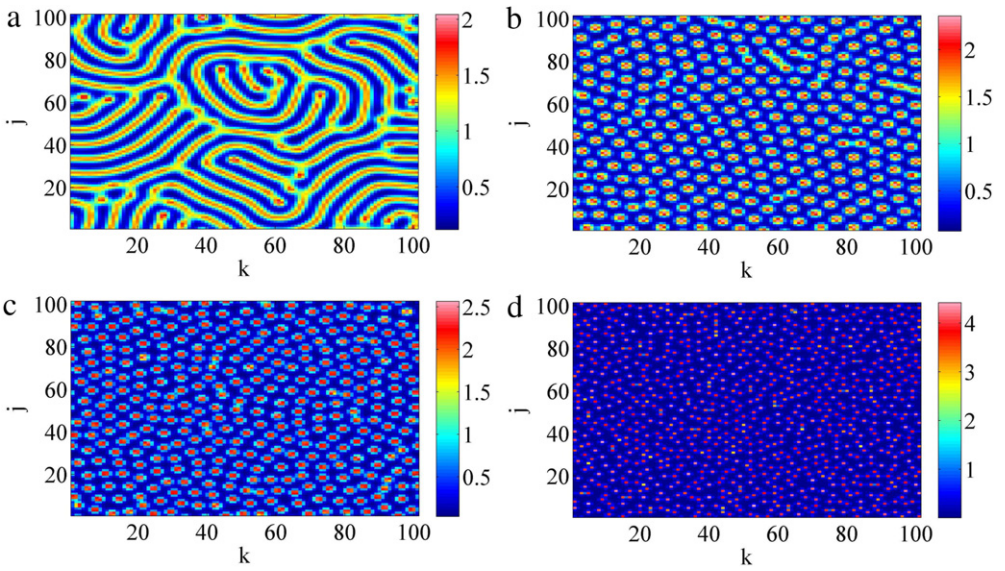

Fig. 4. Spatial patterns for the activator variable (in colorscale) for a two-dimensional square lattice of 101 × 101 cells, for a fixed time, chosen so as to exhibit stationary behavior, with $\alpha = 1000$ and (a) $D_u = 0.016$; (b) 0.014; (c) 0.012; (d) 0.005. (For interpretation of the references to color in this figure legend, the reader is referred to the web version of this article.)

Fig. 4 shows the two-dimensional spatial pattern of the activator concentration (indicated in a colorscale), at a fixed time, for the diffusive coupling case ($\alpha = 1000$), a situation previously investigated by Meinhardt and his collaborators [10]. The value of the activator diffusion coefficient D_u was varied in an interval for which the system is Turing-unstable, such that we focus on the spatial patterns generated after instability saturation by the nonlinear terms in the dynamics. A familiar stripe-like (or "zebra") pattern appears for $D_u = 0.016$, just after the threshold for Turing instability (Fig. 4(a)).

The appearance of such stripe-like patterns is due to the auto-catalysis saturation for high activator concentration values. Since the activator cannot increase further the region of high activator concentration becomes wider. This widening, however, is limited by lateral inhibition caused by neighbor lattice points, what produces stripe-like regions of high activator concentration [10]. These stripe-like patterns become spot-like structures (or "leopard" patterns) when the diffusion coefficient is lower (Fig. 4(b)). Indeed, for lower values of D_u the system does not develop stripes, which require some amount of activator diffusion, and the activated cells tend to be isolated spots whose size decrease if D_u is further lowered (Fig. 4(c)). It is worth observing that, as the spot becomes narrower, its height increases (from ∼2.5 to ∼4.0) (Fig. 4(d)), suggesting a "squeezing" effect on the spots caused by the neighbor inhibitor cells.

A representative example of spatial patterns formed in the case of non-local coupling ($\alpha = 1$) is provided by Fig. 5, for different values of D_u (after the occurrence of a Turing instability). Just after the instability threshold ($D_u = 0.015$) we have a periodic pattern (Fig. 5(a)). An essential difference with the diffusive case, for which stripe-like patterns appear, is that the interaction range now is considerably larger, so the diffusion effect overcomes local inhibition, so leading to the formation of large stripes. In general, periodic patterns typically appear when the range of the inhibitor species is smaller than the size of the reaction domain, what facilitates the formation of regular structures [10]. As we decrease D_u the stripes become spots (Fig. 5(b)) with decreasing size and larger heights, showing that the "squeezing" effect acts for non-local couplings as well (Fig. 5(c) and (d)).

In the global (all-to-all) coupling case ($\alpha = 0$) the Turing instability threshold occurs just before $D_u = 0.011$, for which value the corresponding spatial pattern is depicted in Fig. 6(a). Here the coupling effect spreads so widely over the reaction domain that it favors spatially homogeneous patterns. Due to the local inhibition, however, such a dominating background is punctuated by very narrow and tall spots (Fig. 6(b)). The analysis of the spatio-temporal patterns shown in Figs. 4–6 can be made in a quantitative way as well using suitably defined quantifiers, like a spatial correlation function and spatial recurrence-based diagnostics [21].

5. Conclusions

The diffusively coupled Meinhardt–Gierer equations have been successfully used for describing a wide class of activator–inhibitor systems, with a plethora of applications in physical, chemical, and biological systems. We have explored some possibilities related with a non-local coupling, where each oscillator interacts not only with its nearest-neighbors but also with distant ones. There are at least two systems of practical interest for which the latter description would be applicable.

The first example consists of point-like oscillators, like biological cell clocks, which interact through the release and absorption of a substance which diffuses through the inter-cellular medium. If the diffusion occurs very fast we can adia-

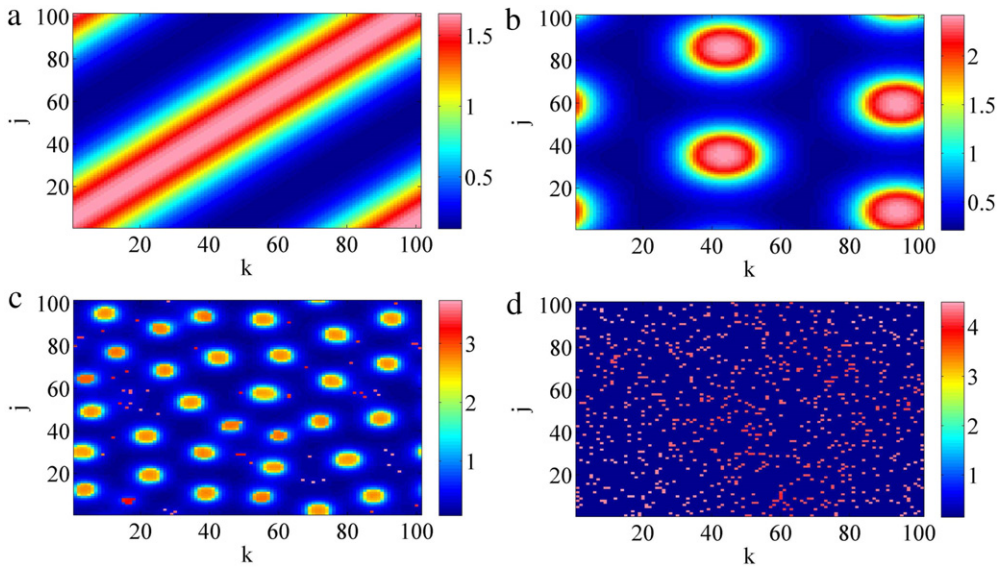

Fig. 5. Spatial patterns for the activator variable (in colorscale) for a two-dimensional square lattice of 101 × 101 cells, for a fixed time, chosen so as to exhibit stationary behavior, with $\alpha = 1.0$ and (a) $D_u = 0.015$; (b) 0.013; (c) 0.011; (d) 0.005. (For interpretation of the references to color in this figure legend, the reader is referred to the web version of this article.)

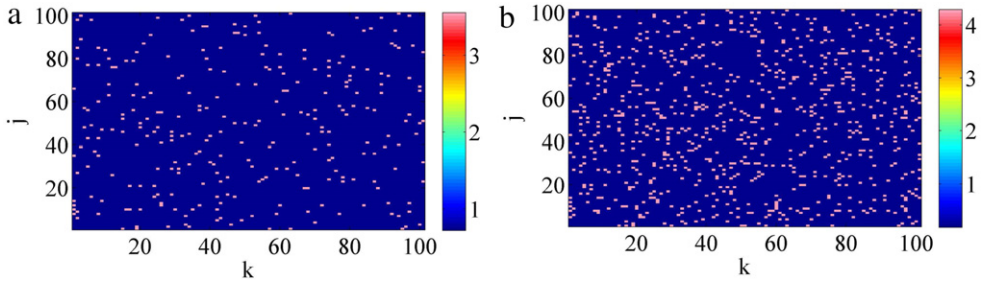

Fig. 6. Spatial patterns for the activator variable (in colorscale) for a two-dimensional square lattice of 101 × 101 cells, for a fixed time, chosen so as to exhibit stationary behavior, with $\alpha = 0$ and (a) $D_u = 0.011$; (b) 0.005. (For interpretation of the references to color in this figure legend, the reader is referred to the web version of this article.)

batically eliminate this third substance and work with a non-locally coupled oscillator system [22,23]. The second example is a neuronal network where each neuron can interact with its neighbors through two kinds of synapses: electrical (gap-junction) synapses, where only the nearest-neighbors are involved due to the necessity of a physical contact between cells; and chemical synapses, which take into account the effect of a number of neurons in an extended vicinity [24]. It is worth mentioning that Turing patterns have been observed in network-organized activator–inhibitor systems [18].

In this paper we considered a non-local coupling version of the spatially extended activator–inhibitor system described by Meinhardt–Gierer equations. In the cases analyzed, the coupling strength decreases with the lattice distance (in two dimensions) as a power-law. We proposed a kind of variable range coupling in which one can pass from a local coupling to a global (all-to-all) coupling by varying the distance exponent. Using linear stability analysis of Fourier spatial modes we obtained conditions for the occurrence of a Turing instability, by which a spatially homogeneous pattern can become unstable. We expressed these conditions in a parameter plane, in which we evaluated the fraction of parameter values yielding instability.

Pattern formation is possible due to the action of nonlinear terms in the system dynamics, since they limit the growth of the linear modes. We have obtained spatial patterns, by numerical integration of the coupled equations, in the cases of diffusive (large exponent), intermediate, and global (small exponent) couplings. The diffusive case presents, just after the occurrence of a Turing instability, stripe-like patterns which appear due to the lateral inhibition. As we depart from the instability threshold, the decreasing effect of diffusion favors the appearance of spot-like patterns, which become narrower and taller (the squeezing effect) as the activator diffusion coefficient decreases.

The formation of stripe-like patterns seems to be a characteristic feature of diffusion couplings, since it was not observed in non-local couplings, where spot-like patterns are chiefly observed as narrow peaks scattered over a homogeneous background. This tendency is more pronounced as more global (all-to-all) is the coupling. In those cases, the squeezing effect in spot-like patterns has been observed as well. The stripes are characterized by a kind of lateral inhibition and are

more likely to occur in the locally coupled case than in the global coupling. The latter are more typically characterized by more or less randomly scattered spots. In the intermediate region we have big spots (clusters) and wavelike patterns.

Acknowledgments

This work was made possible through partial financial support from the following Brazilian research agencies: CNPq and CAPES (PROCAD). The computer simulations were performed at the LCPAD cluster at Universidade Federal do Paraná, acquired thanks to a financial support provided by FINEP (CT-INFRA).

References

[1] M.C. Cross, H. Greenside, Pattern Formation and Dynamics in Non-Equilibrium Systems, Cambridge University Press, 2009.
[2] M.C. Cross, P. Hohenberg, Rev. Modern Phys. 65 (1993) 851.
[3] J.D. Murray, Mathematical Biology, second ed., Springer, Berlin, 1993.
[4] A. Turing, Philos. Trans. R. Soc. Lond. 237 (1952) 37.
[5] Q. Ouyang, H.L. Swinney, Chaos 1 (1991) 411.
[6] I. Lengyel, G. Rábai, I. Epstein, J. Am. Chem. Soc. 112 (1990) 4606;
I. Lengyel, G. Rábai, I. Epstein, J. Am. Chem. Soc. 112 (1990) 9104.
[7] S. Setayeshgar, M.C. Cross, Phys. Rev. E 58 (1998) 4485. 59, 4258 (1999).
[8] A. Gierer, H. Meinhardt, Kybernetik 12 (1972) 30.
[9] A. Gierer, Prog. Biophys. Mol. Biol. 37 (1981) 1.
[10] H. Meinhardt, J.A. Koch, Rev. Modern Phys. 66 (1994) 1481.
[11] H. Meinhardt, Models of Biological Pattern Formation, Academic Press, London, 1982.
[12] S.E.de S. Pinto, S.R. Lopes, R.L. Viana, Physica A 303 (2002) 339.
[13] C. Anteneodo, A.M. Batista, R.L. Viana, Phys. Lett. A 326 (2004) 227.
[14] R.L. Viana, C. Grebogi, S.E.de S. Pinto, S.R. Lopes, A.M. Batista, J. Kurths, Physica D 206 (2005) 94.
[15] R.L. Viana, F.A.dos S. Silva, S.R. Lopes, Phys. Rev. E 83 (2011) 046220.
[16] A.M. Batista, S.E.de S. Pinto, R.L. Viana, S.R. Lopes, Physica A 322 (2003) 118.
[17] E. Atlee-Jackson, Perspectives in Nonlinear Dynamics, Vol. II, Cambridge University Press, Cambridge, 1991.
[18] H. Nakao, A.S. Mikhailov, Nat. Phys. 6 (2010) 544.
[19] R.L. Viana, A.M. Batista, C.A.S. Batista, J.C.A. de Pontes, F.A.S. Silva, S.R. Lopes, Commun. Nonlinear Sci. Numer. Simul. 17 (2012) 2924.
[20] S.H. Strogatz, Nonlinear Dynamics and Chaos, Perseus Books, 1994.
[21] F.A.S. Silva, R.L. Viana, T.L. Prado, S.R. Lopes, Commun. Nonlinear Sci. Numer. Simul. 19 (2014) 1055.
[22] Y. Kuramoto, Progr. Theoret. Phys. 94 (1995) 321.
[23] Y. Kuramoto, H. Nakao, Phys. Rev. Lett. 76 (1996) 4352; Physica D 103 (1997) 294.
[24] C.A.S. Batista, R.L. Viana, F.A.S. Ferrari, S.R. Lopes, A.M. Batista, J.C.P. Coninck, Phys. Rev. E 87 (2013) 042713.